CrystEngComm



PAPER



Cite this: CrystEngComm, 2020, 22, 1112

Complex cobalt silicates and germanates crystallizing in a porous three-dimensional framework structure†

Mohammad Usman, ¹ Mark D. Smith, ¹ Vancho Kocevski, ¹ t^b Theodore Besmann ob and Hans-Conrad zur Love ** **

Four new cesium-containing cobalt oxide complexes were reported. Cs(Co_{0.5}Si_{0.5})SiO₄ (1), $Cs_{1.29(5)}Co_{0.69(5)}Ge_{1.81(5)}O_5$ (2), and its ordered analogue $Cs_2CoGe_4O_{10}$ (3) were synthesized using a mixed CsCl-CsF flux at 850 °C or 900 °C. The structure of (1) closely resembles that of known zeolite and feldspar structures, and (1) crystallizes in the noncentrosymmetric monoclinic space group Im with lattice parameters of a = 8.9926(4) Å, b = 5.4599(2) Å, c = 9.3958(6) Å, and $\beta = 91.5928(18)^\circ$. Complexes (2) and (3) crystallize in the same new structure with a highly porous three-dimensional framework in the tetragonal space group /4 with lattice parameters of a = 7.4239(14) Å and c = 13.169(3) Å for (2) and a = 7.3540(6) Å and c = 13.1122(11) Å for (3). The formation of (2) vs. (3) can be controlled based on slight variations in the quantities of the starting materials. Single-crystal-to-single-crystal ion exchange of (1) in a molten RbNO₃ bath resulted in 14% Cs exchange with Rb, affording the composition $Cs_{0.86}Rb_{0.14}(Co_{0.5}Si_{0.5})SiO_4$ (4). Firstprinciples density functional theory calculations were performed to elucidate the electronic and magnetic properties and stabilities of (1) and (3) at 0 K.

Received 21st October 2019, Accepted 9th January 2020

DOI: 10.1039/c9ce01662g

rsc.li/crystengcomm

1. Introduction

Quaternary alkali cobalt silicates and germanates are scarce, and most that have been reported were structurally characterized based on powder X-ray diffraction data. 1-4 Among reported silicates, only three quaternary Cs/Co/Si/O phases have been deposited in the ICSD database: Cs2CoSiO4, Cs₅CoSiO₆, and Cs₂CoSi₅O₁₂.^{4,5} In these mixed cobalt silicates, the substantial size difference between Co^{3+} (r = 0.545 Å, low spin octahedral coordination) and Si^{4+} (r = 0.26 Å, tetrahedral coordination) should ensure that no site mixing occurs between cobalt and silicon; surprisingly, Co3+/Si4+ site mixing is nonetheless observed in Cs5CoSiO6, which features two Co/Si mixed-metal sites. In contrast, no site mixing is typically observed in Co²⁺-containing silicates. For example, Cs₂CoSiO₄

Interest in this class of materials arises from the ability to prepare members of this family of silicates with noncentrosymmetric structures, making these materials potentially second harmonic generation active and hence of interest for applications based on non-linear optical properties. To date, no reported quaternary Cs/Co/Ge/O systems have been structurally characterized by single-crystal X-ray diffraction, although a number of ternary cobalt germanates have been observed, including CoGeO₃, Co₁₀Ge₃O₁₆, and Co₂GeO₄.⁶⁻⁸ Hence, the ability to obtain these phases in single-crystal form is highly desirable as it can greatly improve their structural characterization (vide infra). During crystal growth, it is generally accepted that an ordered vs. disordered structure (in this case, the presence or absence of Co/Ge site mixing) is influenced by the thermodynamic stability of different site occupancies and by the speed of crystal formation. Representative examples of this are two of the phases discussed in this paper, $Cs_{1.29(5)}Co_{0.69(5)}Ge_{1.81(5)}O_5$ (2) and its ordered analogue Cs₂CoGe₄O₁₀ (3), which are isostructural but differ in the presence of Co/Ge site mixing.

features ordered Co and Si sites. This may reasonably be attributed to the large ionic size of Co^{2+} (r = 0.58 Å, high spin tetrahedral coordination) in addition to the large charge difference between the Co (+2) and Si (+4). In this work, we introduce another example, Co(II)-containing Cs₂CoSi₃O₈, that features both, two unique silicon sites and two mixed Co(II)/Si sites.

^a Department of Chemistry and Biochemistry, University of South Carolina, Columbia, SC 29208, USA. E-mail: zurloye@mailbox.sc.edu

^b Department of Mechanical Engineering, University of South Carolina, Columbia, South Carolina 29208, USA

[†] Electronic supplementary information (ESI) available: An extended discussion of the crystallographic refinements for (1)-(3), single-crystal optical images, and scanning electron microscopy and EDS results. CCDC 1905091 (1), 1905090 (2), 1957759 (3), and 1957758 (4). For ESI and crystallographic data in CIF or other electronic format see DOI: 10.1039/c9ce01662g

[‡] Current address: MST-8, Los Alamos National Laboratory, Los Alamos, NM 87545, USA.

CrystEngComm Paper

We successfully explored the molten cesium halide flux crystal growth and prepared three new, complex cobalt silicates and germanates. Herein, we report the synthesis of (1)–(3), density functional theory (DFT) calculations, and the formation of the ion-exchange product of (1), $Cs_{0.86}Rb_{0.14}(Co_{0.5}Si_{0.5})SiO_4$ (4).

2. Experimental section

2.1. Reagents

 CoF_2 (Alfa Aesar, anhydrous powder, 98%), SiO_2 (Alfa Aesar, 99.9%), GeO_2 (99.999%, Alfa Aesar), RbCl (Alfa Aesar, 99.8%), RbF (99.1%, Alfa Aesar), RbNO₃ (Alfa Aesar, 99.8%), CsCl (Ultra-pure, VWR), and CsF (Alfa Aesar, 99.9%) were used as received without further modification for the synthesis of all title compounds.

2.2. Flux growth

Single crystals of the title compounds were obtained via mixed CsCl-CsF flux growth. In general, the compounds were synthesized by charging a cylindrical silver crucible with dimensions of 7.5 cm (height) by 1.2 cm (diameter). One end of the crucible was sealed and welded shut using a TIG-175 Square Wave Lincoln electric welder with CoF2, TO2 (T = Si, Ge), and the appropriate amount of CsCl-CsF flux. The specific amounts of the reagents and the flux along with the details of the heating and cooling cycle are listed in Table 1. The tube containing the charge was placed into a programmable furnace and heated to the reaction temperature, held at this temperature for the desired number of hours, and then slowly cooled to well below the melting point of the flux, at which point the furnace was turned off. In all three cases, deep-blue crystals with different morphologies were obtained by dissolving the solidified flux in warm distilled water under sonication and then washing the crystals with acetone during vacuum filtration. The typical yield was less than 25%.

2.3. Energy-dispersive spectroscopy (EDS)

Elemental analysis was performed on single crystals of all compounds using a TESCAN Vega-3 SBU scanning electron microscope with EDS capabilities. Single crystals of (1)–(4) were mounted on carbon tape, and EDS was carried out using a 20 kV accelerating voltage and an accumulation time of 20 s. EDS verified the presence of the appropriate elements in

all compositions. The absence of extraneous elements in the product crystals (*e.g.*, silver from the reaction vessel) was confirmed within the detection limits of the instrument. The results of semi-quantitative elemental analyses are provided in the ESI.†

2.4. Ion exchange

Single-crystal-to-single-crystal ion exchange reactions were performed on (1) by layering 0.1 g of crystals under 1 g of RbNO $_3$ in a fused-silica ampoule measuring 7.5 cm in length. The tube containing the charge was heated at 350 °C for 16 h. Once the reaction was complete, the flux was dissolved in hot water, and the crystals were thoroughly rinsed and examined by single-crystal X-ray diffraction.

2.5. Single-crystal X-ray diffraction

X-ray intensity data from suitable crystals of (1)–(4) were collected at 301(2) K using a Bruker D8 QUEST diffractometer equipped with a PHOTON 100 CMOS area detector and an Incoatec microfocus source (Mo K α radiation, λ = 0.71073 Å). The raw area detector data frames were reduced and corrected for absorption effects using the SAINT+ and SADABS programs. Thit is structural models were obtained with SHELXT. Subsequent difference Fourier calculations and full-matrix least-squares refinement against F^2 were performed with SHELXL-2018 using the ShelXle interface for (2) and (3) and OLEX2 for (1) and (4). Crystallographic data, refinement data, and interatomic distances for all compounds are listed in Tables 2–6. A detailed crystallographic discussion is provided in the ESI.†

2.6. First-principles calculations

First-principles density functional theory (DFT) calculates were performed with an on-site Coulomb interaction (*i.e.*, DFT+*U*) using the Vienna *ab initio* package (VASP), ^{14,15} the projector augmented wave (PAW) method, ^{16,17} and the generalized gradient approximation of Perdew, Burke, and Ernzerhof (PBE). ¹⁸ To model Si/Co mixing and the partial occupancies of Cs atom in (1) and (3), super quasi-random structures (SQSs) were made (relaxed SQSs are given in the ESI†). Structures (2) and (4) could not be reproduced because reproducing the low Co and Rb concentrations requires a huge SQS (>1000 atoms), making the calculations prohibitively expensive. To see if (1) and (3) are thermodynamically

Table 1 Reagents and reaction conditions for (1)–(4).

Compound	Reagents	Flux	Temperature profile
(1)	1 mmol CoF ₂	1.85 g CsCl	Heated at 600 $^{\circ}$ C h $^{-1}$ to 900 $^{\circ}$ C, held for 12 h, and slowly cooled to 400 $^{\circ}$ C at 6 $^{\circ}$ C h $^{-1}$
	1 mmol SiO ₂	1.36 g CsF	
(2)	1 mmol CoF ₂	3.15 g CsCl	Heated at 300 °C h ⁻¹ to 850 °C, held for 24 h, and slowly cooled to 400 °C at 6 °C h ⁻¹
	4 mmol GeO ₂	2.31 g CsF	
(3)	1 mmol CoF ₂	1.85 g CsCl	Heated at 300 °C h ⁻¹ to 850 °C, held for 24 h, and slowly cooled to 400 °C at 6 °C h ⁻¹
	2 mmol GeO ₂	1.36 g CsF	
(4)	0.1 g compound (1)	1 g RbNO ₃	Heated at 600 °C h ⁻¹ to 350 °C, held for 16 h, and shut off

Paper CrystEngComm

Table 2 Crystallographic and refinement data for (1)-(4)

Compound	(1)	(2)	(3)	(4)
Empirical formula	$CsCo_{0.50}Si_{1.50}O_{4}$	Co _{0,69} Cs _{1,29} Ge _{1,81} O ₅	Cs ₂ CoGe ₄ O ₁₀	Cs _{0.86} Rb _{0.14} Co _{0.50} Si _{1.50} O ₄
Crystal color and habit	Blue plate	Deep blue irregular	Deep blue block	Blue block
F.W. (g mol ⁻¹)	268.51	423.02	775.13	261.73
Crystal system	Monoclinic	Tetragonal	Tetragonal	Monoclinic
Space group	Im	$Iar{4}$	$Iar{4}$	Im
a (Å)	8.9926(4)	7.4239(14)	7.3540(6)	8.996(2)
$b(\mathring{A})$	5.4599(2)	13.169(3)	13.112(1)	5.4500(10)
c (Å)	9.3958(6)	13.169(3)	13.112(1)	9.381(2)
β (°)	91.5928(18)	90	90	90.709(17)
Z	4	4	2	4
$V(\mathring{A}^3)$	461.14(4)	725.8(3)	709.13(13)	459.89(17)
$\rho_{\rm calc.} ({\rm mg \ m}^{-3})$	3.868	3.871	3.630	3.780
Crystal size (mm ³)	$0.06 \times 0.03 \times 0.02$	$0.20 \times 0.14 \times 0.10$	$0.16 \times 0.12 \times 0.10$	$0.10 \times 0.08 \times 0.07$
Flack parameter	0.50(7)	0.046(7)	0.013(7)	a
Goodness of fit on F^2	1.150	1.062	1.221	1.091
Final R indices $[I > 2 \text{sigma}(I)]$	$R_1 = 0.0209$	$R_1 = 0.0206$	$R_1 = 0.0235$	$R_1 = 0.0309$
Final R indices (all data)	$WR_2 = 0.0428$	$WR_2 = 0.0514$	$wR_2 = 0.0661$	$WR_2 = 0.0741$
Largest diff. peak and hole (e A)	0.757/-0.556	0.460/-0.368	0.712/-0.372	1.727/-1.126

^a Twinning involves inversion, so the Flack parameter could not be determined.

stable (i.e., if they break the Cs-Co-Si-O and Cs-Co-Ge-O convex hulls, respectively), their formation energies were compared with respect to the Open Quantum Materials Database (OOMD). 19 The OOMD calculation setup was as follows: 520 eV cut-off energy for the plane-wave basis set; 10⁻⁴ eV energy convergence criterion; $6 \times 9 \times 5$ and $7 \times 7 \times 4$ k-point meshes for (1) and (3), respectively; and $U_{\text{eff}} = 3.3$ eV for the Co atoms. The system was considered to be spin-polarized with high-spin ferromagnetic (FM) and antiferromagnetic (AFM; magnetic moment = $0\mu_{\rm B}$) ordering of the Co atoms.²⁰ For calculating the electronic and optical properties, more rigorous calculations were performed using a 520 eV cut-off energy for the plane wave basis set, energy and force convergence criteria of 10⁻⁶ eV and 10⁻³ eV Å⁻¹, respectively, and the same k-point meshes as in the OQMD calculations. The ground-state geometry was obtained by relaxing the cell volume, cell shape, and atomic positions. The adsorption indices of (1) and (3) were obtained from the calculated frequency-dependent dielectric function in the independentparticle picture.

Table 3 Selected interatomic distances (Å) for (1). M(1) and M(2) = 50/50Co/Si

	Exp.	DFT	Error
$M(1)-O(2) \times (2)$	1.821(16)	1.9299 Co-O	
M(1)-O(3)	1.893(10)	1.9540 Co-O	
M(1)-O(5)	2.012(11)	1.9551 Co-O	
M(2)-O(5)	1.405(10)	1.5833 Si-O	
M(2)-O(6)	1.707(10)	1.6271 Si-O	
$M(2)-O(1) \times (2)$	1.781(17)	1.6684 Si-O	
Si(1)-O(3)	1.550(10)	1.5865	2.35%
$Si(1)-O(1)\times(2)$	1.572(17)	1.6015	1.88%
Si(1)-O(4)	1.680(12)	1.6720	-0.48%
Si(2)-O(4)	1.592(11)	1.6433	3.2%
$Si(2)-O(2)\times (2)$	1.630(16)	1.6593	1.80%
Si(2)-O(6)	1.670(11)	1.6695	-0.03%

3. Results and discussion

3.1. Synthesis

Mixed-alkali fluoride-chloride melts have been remarkably successful for crystallizing complex silicates germanates²¹ and were used to obtain single crystals of the title compounds: $Cs(Co_{0.5}Si_{0.5})SiO_4$ (1), $Cs_{1.29(5)}Co_{0.69(5)}Ge_{1.81(5)}$ -O₅ (2), and Cs₂CoGe₄O₁₀ (3). However, none of the crystal growth reactions described herein yielded a phase-pure product, and numerous attempts to obtain a phase-pure product by adjusting the temperature, reagent ratios, and so on failed. Due to the small sizes of the crystals, it was not possible to pick a phase-pure sample of any of the title compounds. In addition, attempts to synthesize (1) and (3) via a solid-state approach did not result in a phase-pure product. In both cases, obtaining a pristine sample for measurements of physical properties was prevented by the formation of undesired phases (Cs2CoSi5O12 and Cs2CoGe5O12). The solidstate synthesis of Cs2CoSi5O12 was carried out to determine its magnetic properties, which have not been reported to date. The compound is a simple Curie paramagnet in the entire range of 2-375 K with no obvious magnetic ordering down to 2 K.

It is fascinating to observe how different amounts of reagents subjected to similar reaction conditions can lead to order and disorder in the same crystal structure. For

Table 4 Selected interatomic distances (Å) for (2). M(1) = Ge(1)/Co(1A) = 0.867/0.133 and M(2) = Co(1)/Ge(1A) = 0.85(4)/0.15(4)

M(1)-O(2)	1.723(4)
M(1)-O(1)	1.755(4)
M(1)-O(3)	1.760(3)
M(1)-O(1)	1.761(4)
$M(2)-O(2) \times (4)$	1.926(4)

CrystEngComm **Paper**

Table 5 Selected interatomic distances (Å) for (3)

	Exp.	DFT	Error
$Co(1)-O(2) \times (4)$	1.948(4)	1.9796	1.62%
Ge(1)-O(1)	1.742(4)	1.7813	2.25%
Ge(1)-O(1)	1.762(3)	1.8035	2.35%
Ge(1)-O(2)	1.706(4)	1.7216	0.91%
Ge(2)-O(3)	1.760(3)	1.7954	2.01%

Table 6 Selected interatomic distances (Å) for (4). M(1) and M(2) = 50/50 Co/Si

$M(1)-O(2) \times (2)$	1.88(2)
M(1)-O(3)	1.897(17)
M(1)-O(5)	1.98(2)
M(2)-O(5)	1.38(2)
M(2)-O(6)	1.722(17)
$M(2)-O(1)\times(2)$	1.70(2)
Si(1)-O(3)	1.532(18)
$Si(1)-O(1) \times (2)$	1.63(2)
Si(1)-O(4)	1.68(2)
$\operatorname{Si}(2)$ -O(4)	1.60(2)
$Si(2)-O(2)\times(2)$	1.59(2)
Si(2)-O(6)	1.67(2)
* * * * * * * * * * * * * * * * * * * *	. ,

instance, (2), which contains only mixed Co and Ge sites, can be prepared by layering 1 mmol of CoF₂ and 4 mmol of GeO₂ under 3.15 g of CsCl and 2.31 g of CsF. Decreasing the amount of GeO2 to 2 mmol and the amounts of CsCl and CsF to 1.85 g and 1.36 g, respectively, yields (3), which contains only ordered, fully occupied Co and Ge sites and is isostructural to (2). In contrast, (1) can be synthesized by using either 1 mmol or 2 mmol of SiO2; however, the crystal quality is worse when 2 mmol of SiO2 is used. Further increases in the amount of SiO₂ leads to the formation of Cs₂CoSi₅O₁₂.⁵ Similar reactions were also carried out using molten RbCl-RbF flux, leading to the formation of compounds displaying even higher structural complexity than the phases reported herein; these compounds will be reported elsewhere.

3.2. Crystal structure and ion exchange

Structure (1) crystallizes in the monoclinic system in space group Im. The asymmetric unit consists of two Cs atoms, two Si atoms, two mixed sites modeled as 50/50 Co/Si, and six unique oxygen atoms. The crystal structure of (1) is characteristic of the '1114' family of transition metal-based lithium aluminosilicates.²² Members of this family crystallize in a wide variety of space groups: NaCoPO₄ (P6₁), KCoPO₄ (P6₃), NH₄CoPO₄ (P6₃), RbCoPO₄ (P2₁), and TlZnAsO₄ $(P2_1)$. 23,24 The ABW 22 zeolite topology has been extensively studied previously and consists of six-ring sheets and zigzag chains.^{25,26} Usually, the ABTO₄-type zeolites (A = alkali metal, B = divalent or trivalent metal, X = P, Si, or Ti) feature either ordered, alternating BO₄ and TO₄ tetrahedral frameworks, as observed in CsFeSiO4, or a disordered framework, as observed in CsAlTiO₄, in which the tetrahedral sites

exhibit mixed Al/Ti occupancies. 26,27 As seen from its structural formula, Cs(Co_{0.5}Si_{0.5})SiO₄ (1) is a rare example that features two unique Si sites along with two mixed-metal sites that are 50/50 occupied by Co/Si. The crystal structure of (1) is comprised of corner-sharing Co(1)/Si(1A) and Co(2)/ Si(2A) tetrahedral dimers bridged by the disordered O(5) that alternate with Si(1)O4 and Si(2)O4 pyrosilicate units via corner-sharing such that the resulting (Co/Si)O4 and SiO4 network features large eight-sided cavities running down the b-axis and relatively smaller, nearly perfect hexagonal (sixmembered) channels running down the a-axis. These cavities and channels crisscross the crystal framework in all three directions and are occupied by fully ordered Cs cations that provide charge balance to the anionic cobaltosilicate framework. The Co(1)/Si(1A)-O and Co(2)/Si(2A)-O bond distances range from 1.821(16)-2.012(11) Å and 1.405(10)-1.781(17) Å, respectively. The unusually short Co-O distance of 1.405(10) Å can, at best, be attributed to the extensive disorder in the structure and is likely an artefact of the moderate crystallinity of the available sample. The Si-O bond lengths in the Si(1)O₄ and Si(2)O₄ tetrahedra range from 1.550(10)-1.680(12) Å and 1.592(11)-1.670(11) Å, respectively, in good agreement with the typical value of ~1.64 Å for average Si-O bond lengths. Fig. 1 illustrates the crystal structure of (1).

To determine if the Cs ions in the channels can be ion-exchanged, single crystals of (1) were soaked in a molten RbNO₃ bath at 350 °C. The Cs ions underwent partial exchange, and the product phase, Cs_{0.86}Rb_{0.14}Co_{0.5}Si_{1.5}O₄ (4), contained 14% Rb and 86% Cs, as determined by singlecrystal X-ray diffraction. The cobaltosilicate framework structure was unchanged by the ion-exchange process. The

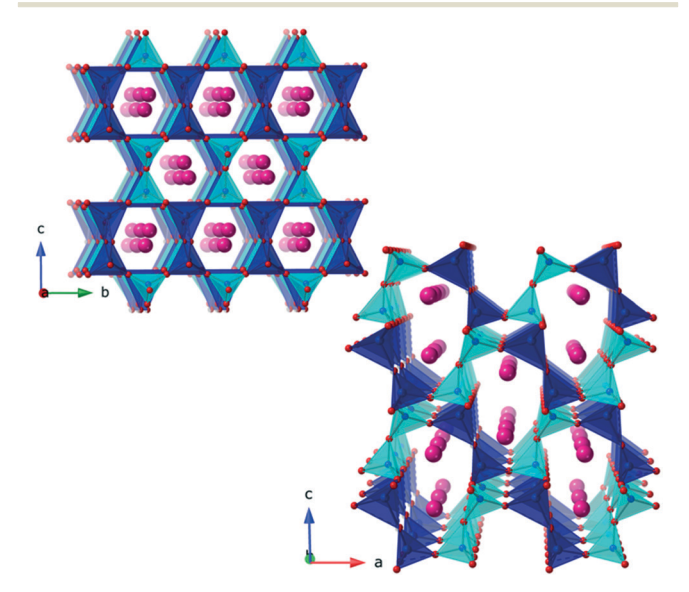


Fig. 1 The crystal structure of (1) featuring hexagonal (six-membered) channels down the a-axis (top) and eight-sided cavities down the b-axis (bottom). The mixed (50/50) Co/Si sites are shown in deep blue, while pure Si sites are shown in turquoise. Cs and O are depicted as pink and red spheres, respectively.

Paper CrystEngComm

presence of Rb in ion-exchanged crystals was further corroborated by semi-quantitative EDS analysis.

The asymmetric unit of (2) consists of two unique mixed Co/Ge sites, Ge(1)/Co(1A) and Co(1)/Ge(1A), three unique oxygen atoms, and a disordered distribution of electron density modeled as Cs atoms, most on general positions. The asymmetric unit of (3) consists of one Ge atom, one Co atom, three oxygen atoms, and a disordered distribution of electron density modeled as Cs atoms, most on general positions, similar to (2). Structures (2) and (3) are isostructural and only differ in the degree of metal site mixing. For that reason, only the crystal structure of (3), which contains fully ordered Co and Ge sites, is described here. Compound (3) crystallizes in the tetragonal system in space group I4. The crystal structure of (3) consists of a three-dimensional, porous network of corner-sharing CoO₄ and GeO₄ tetrahedra that form large cavities occupied by severely disordered Cs cations, which provide charge balance to the cobaltogermanate framework. The three-dimensional framework consists of two-dimensional sheets of GeO4 tetrahedra lying in the ab-plane. The corner-sharing GeO4 tetrahedra exclusively form dimers, with each dimer running along either the a- or b-axis and corner-sharing with four perpendicular dimers. This assembly of GeO₄ tetrahedra produces infinite two-dimensional sheets that are connected to each other via corner-sharing with CoO4 tetrahedra along the

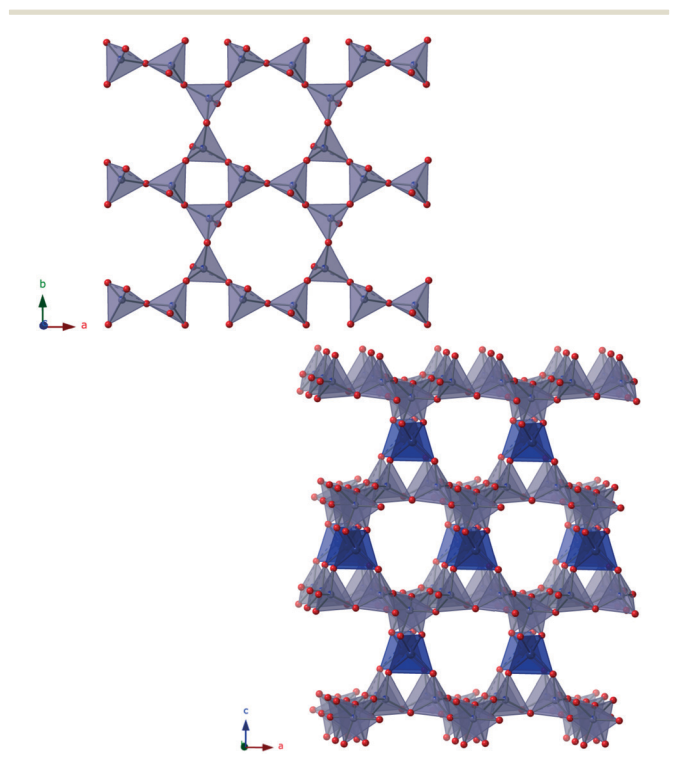


Fig. 2 An illustration of the two-dimensional GeO₄ anionic sheet down the c-axis (top) and the assembly of the two-dimensional sheets into a three-dimensional cobaltogermanate framework (bottom) in (3). Ge and Co sites are shown in lavender and deep blue, respectively. Oxygen is shown in red.

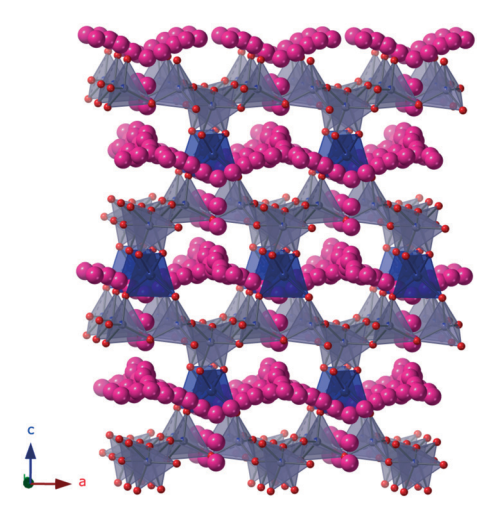


Fig. 3 A polyhedral representation of (3). Ge and Co sites are shown in lavender and deep blue, respectively. Oxygen is shown in red. Cs is shown in pink.

c-axis. This structural arrangement is identical to the allaluminate sheet topology that we recently reported for Cs₂(UO₂)Al₂O₅.²⁸ Each pair of alternating layers in (3) is connected by CoO₄ tetrahedra that corner-share with adjacent, up-facing (UU) GeO4 tetrahedra of the bottom layer and adjacent, down-facing (DD) GeO4 tetrahedra of the top layer (Fig. 2). The Ge-O bond lengths in the GeO4 tetrahedra are 1.706(4)-1.762(3) Å, whereas each CoO₄ tetrahedral unit is comprised of four equal bond lengths of 1.948(4) Å. Fig. 3 shows the crystal structure of (3).

Interestingly, under similar reaction conditions (Table 1), two isostructural materials, (2) with and (3) without Co/Ge site mixing, were obtained. The difference in the synthetic conditions lies solely in the relative amounts of reagents used. When starting with a 1:4 CoF₂/GeO₂ ratio, Co/Ge site mixing was obtained; when starting with a 1:2 CoF₂/GeO₂ ratio, no Co/Ge site mixing was observed. One can speculate that the disordered phase (2) results from a fast crystalgrowth process that incorporates, at random, either Co or Ge into the crystallographic site. In the case of (3), we propose that the growth process is slower, enabling the selective filling of crystallographic sites by either all Co or all Ge. If we assume that the dissolution of GeO₂ is slow, the presence of an increased amount of GeO2 relative to CoF2 can result in a higher solution concentration of Ge in a shorter amount of time, ultimately leading to accelerated crystal growth. The size difference between Co(II) and Ge(IV) should not lead to

Table 7 DFT-calculated crystallographic data for (1) and (3)

	State	$V\left(\mathring{\mathbf{A}}^{3}\right)$	a (Å)	b (Å)	c (Å)	β (°)
(1)	FM	453.40	8.8325	5.4023	9.5050	91.3957
	AFM	451.58	8.8036	5.3878	9.5226	91.1401
(3)	FM	661.58	7.2156	7.2156	12.7067	90
	AFM	661.31	7.2150	7.2150	12.7038	90

CrystEngComm Paper

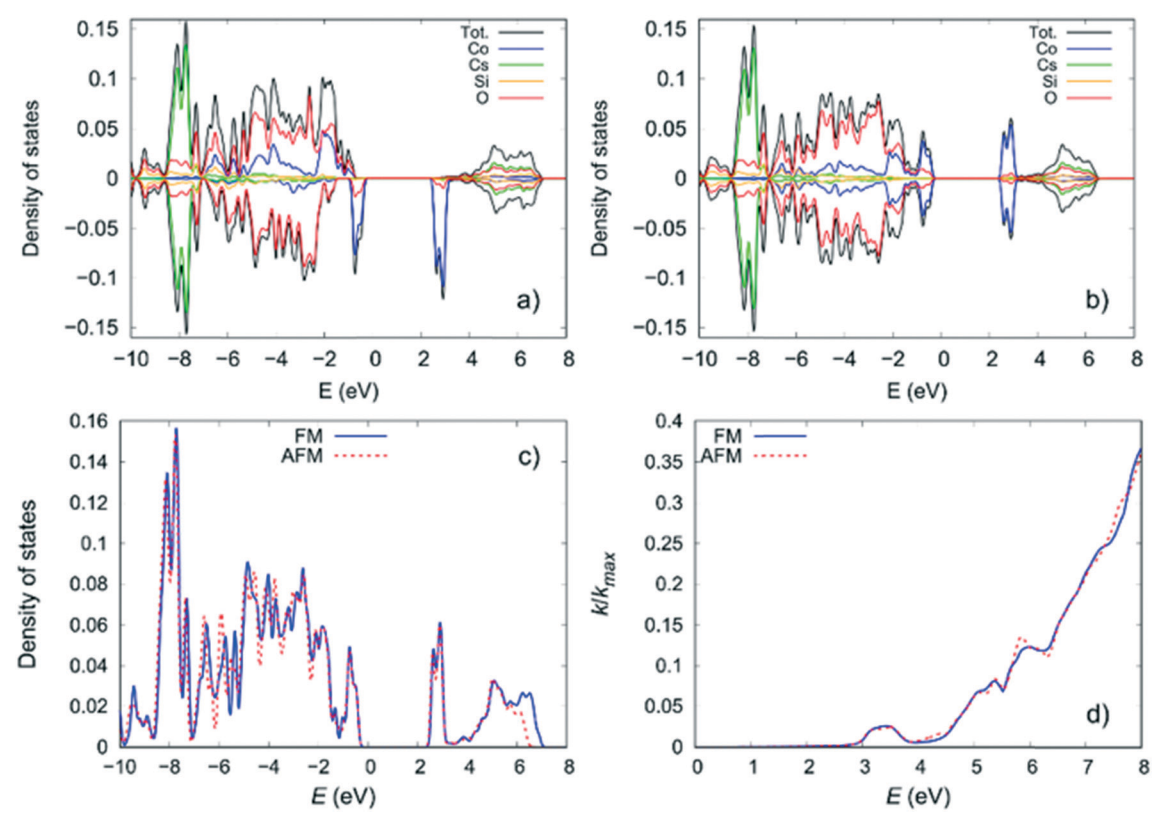


Fig. 4 The projected density of states (PDOS) of (1) for the (a) ferromagnetic (FM) and (b) antiferromagnetic (AFM) states of $Cs(Co_{0.5}Si_{0.5}Si_{0.5})SiO_4$. The total DOS, Co, Cs, Si, and O PDOS are shown in black, blue, green, orange, and red, respectively. (c) Total DOS and (d) absorption indices of $Cs(Co_{0.5}Si_{0.5})SiO_4$ in the FM (blue) and AFM (red) states.

site mixing since both the size difference and charge difference should favor unique crystallographic conditions, as observed for (3). As the heating rates and temperatures were identical, the speed of crystal growth is the remaining parameter that is likely responsible for the presence or absence of site mixing.

3.3. First-principles calculations

Compared to the experimental values for (1) and (3), the calculated lattice parameters of both FM and AFM systems are well reproduced by DFT, with error <3% (see Table 7). Similarly, the total energies of the FM and AFM systems for both (1) and (3) are very similar, with the energy of the FM system being more negative by 1 meV per atom. Both (1) and (3) break the OQMD convex hull by 32 and 175 meV per atom, respectively, indicating that the formations of these compound are energetically favorable. Fig. 4 shows the projected density of states (DOS) of (1) in the FM and AFM systems. The FM DOS has two distinct bandgaps of 3.44 and 3.01 eV in the spin-up and spin-down channels, respectively, while the AFM DOS has only one bandgap of 3 eV. The projected DOS (PDOS) values show that the states around the bandgap in (1) come predominantly from the Co atoms, signifying that Cs(Co_{0.5}Si_{0.5})SiO₄ is a Mott insulator, as is CoO.²⁹ Similarly, the FM DOS of (3) has two band

gaps of 2.52 and 2.07 eV in the spin-up and spin-down channels, respectively, while the AFM DOS has only one bandgap of 2.11 eV (Fig. 5c). However, unlike (1), the states at the bottom of the conduction band of (3) come from the O atoms, while the states at the top of the valence band come from Co (Fig. 5a and b), making $Cs_2CoGe_4O_{10}$ a charge-transfer insulator.

Following the similarity in the structures of (1) and (3), their DOS are also similar. Interestingly, the Co PDOS are almost at the same position in both (1) and (3), while the PDOS of Ge and O are pushed closer to the bandgap in (3). This shift in the PDOS toward the bandgap comes from the higher energy of the Ge valence electrons $(4s^24p^2)$ in (3) compared to the energy of the Si valence electrons (3s²3p²) in (1). According to molecular orbital theory, the higher energy of the Ge valence electrons gives rise to Ge-O hybridized states at higher energy in the valence band and lower energy in the conduction band, thus moving the Ge and O states closer to the bandgap. However, there is one more Ge atom in the formula unit of (3) (Cs₂CoGe₄O₁₀) compared to Si atoms in the formula unit of (1) (Cs₂CoSi₃O₈); this difference has little influence on the position of the PDOS. Despite the different magnetic properties, the total DOS of the FM and AFM systems of (1) and (3) are similar (Fig. 4d and 5d), giving rise to similar absorption indices. On the other hand, the main difference between the adsorption indices

Paper CrystEngComm

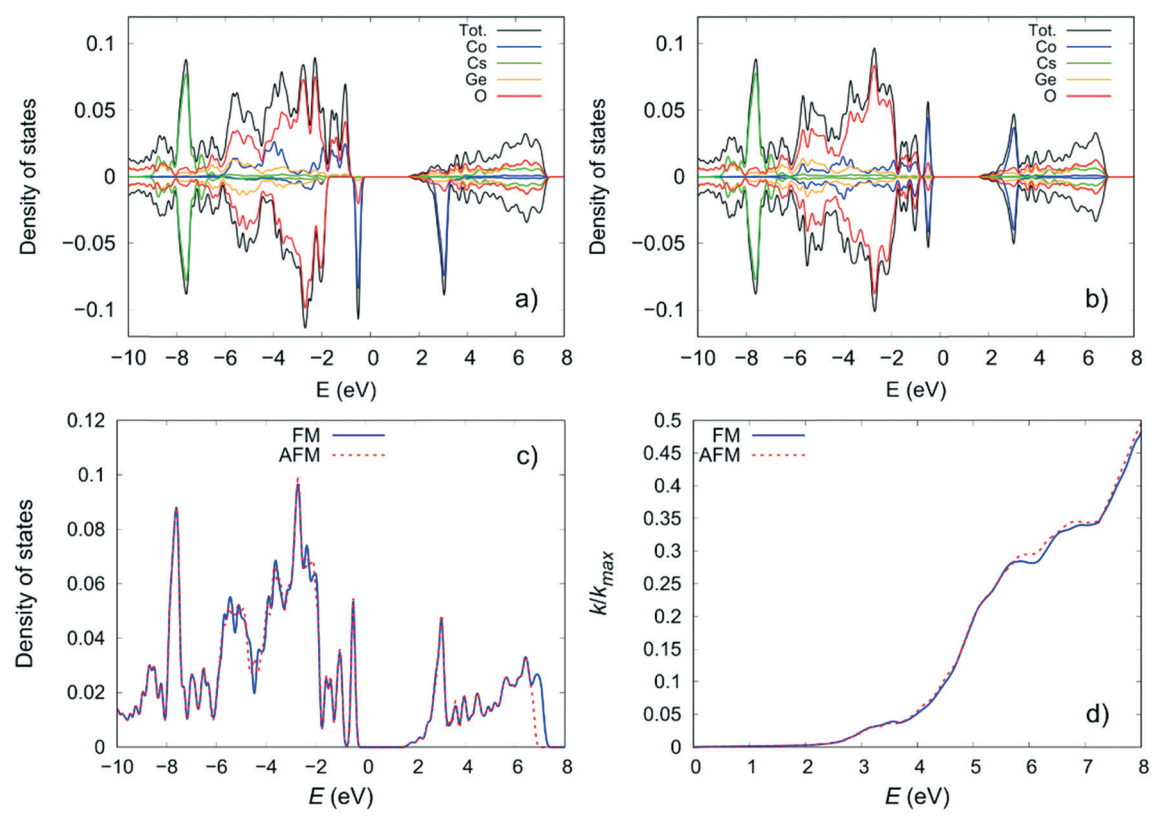


Fig. 5 Projected density of states (PDOS) of (3) in the (a) ferromagnetic (FM) and (b) antiferromagnetic (AFM) states of Cs₂CoGe₄O₁₀. The total DOS, Co, Cs, Ge, and O PDOS are shown in black, blue, green, orange, and red, respectively. (c) Total DOS and (d) absorption indices of Cs₂CoGe₄O₁₀ in the FM (blue) and AFM (red) states.

of (1) and (3) is the small peak at 3.4 eV in (1), which comes from the Co-Co transitions.

4. Conclusions

Using molten cesium halide flux crystal growth, we have synthesized and structurally characterized a new cobaltcontaining cesium silicate, Cs(Co_{0.5}Si_{0.5})SiO₄ (1), and two new cobalt-containing germanates, $Cs_{1.29(5)}Co_{0.69(5)}Ge_{1.81(5)}O_5$ (2) and Cs₂CoGe₄O₁₀ (3). The cesium ions in the cesium cobalt silicate can be partially ion-exchanged for rubidium by soaking the crystals in molten RbNO₃. All compounds crystallize in structures featuring three-dimensional frameworks containing channels occupied by monovalent alkali ions. Semi-quantitative elemental analyses confirmed the presence of all elements in the reported compositions. First-principles DFT calculations indicated that the formations of (1) and (3) are energetically favorable, with the FM state being slightly more stable than the AFM state in both compounds. The DOS indicate that (1) is a Mott insulator, similar to CoO, while (3) is a charge-transfer insulator.

Conflicts of interest

There are no conflicts to declare.

Acknowledgements

M. U., M. D. S., and H. Z. L. performed the syntheses and structural characterization. The authors gratefully acknowledge the U.S. National Science Foundation for supporting this research through grant OIA-1655740. V. K. and T. M. B. acknowledge support from the U.S. Department of Energy, Office of Science, Basic Energy Sciences, under Award No. DE-SC0016574 (Center for Hierarchical Waste Form Materials). This research used computational resources provided by the National Energy Research Scientific Computing Center and the high-performance computing cluster Hyperion supported by The Division of Information Technology at the University of South Carolina.

References

- 1 H. Yamaguchi, K. Akatsuka, M. Setoguchi and Y. Takaki, Acta Crystallogr., Sect. A: Cryst. Phys., Diffr., Theor. Gen. Crystallogr., 1979, 35, 2680.
- 2 W. A. Dollase, Powder Diffr., 1996, 11, 51.
- 3 G. Durand, S. Vilminot, M. Richard-Plouet, A. Derory, J. P. Lambour and M. Drillon, J. Solid State Chem., 1997, 131, 335-340.
- 4 J. Hansing and A. Möller, J. Solid State Chem., 2001, 162, 204-213.

CrystEngComm **Paper**

5 A. M. T. Bell and C. M. B. Henderson, Acta Crystallogr., Sect. C: Cryst. Struct. Commun., 1996, 52, 2132-2139.

- 6 D. R. Z. Peacor, Kristallografiya, 1968, 126, 299-306.
- 7 J. Barbier, Acta Crystallogr., Sect. C: Cryst. Struct. Commun., 1995, 51, 343-345.
- 8 K. Hirota, M. Ohtani, N. Mochida and A. Ohtsuka, J. Ceram. Soc. Jpn., 1989, 97, 8-15.
- 9 APEX3 Version 2016, 5-0 and SAINT+ Version 8.37A, Bruker AXS, Inc., Madison, Wisconsin, USA, 2016.
- 10 L. Krause, R. Herbst-Irmer, G. M. Sheldrick and D. Stalke, J. Appl. Crystallogr., 2015, 48, 3-10.
- 11 (a) G. M. Sheldrick, Acta Crystallogr., Sect. A: Found. Adv., 2015, 71, 3-8; (b) G. M. Sheldrick, Acta Crystallogr., Sect. C: Struct. Chem., 2015, 71, 3-8.
- 12 C. B. Hübschle, G. M. Sheldrick and B. Bittrich, J. Appl. Crystallogr., 2011, 44, 1281-1284.
- 13 O. V. Dolomanov, L. J. Bourhis, R. J. Gildea, J. A. K. Howard and H. Puschmann, J. Appl. Crystallogr., 2009, 42, 339-341.
- 14 G. Kresse and J. Furthmüller, Phys. Rev. B: Condens. Matter Mater. Phys., 1996, 54, 11169-11186.
- 15 G. Kresse and J. Furthmüller, Comput. Mater. Sci., 1996, 6, 15-50.
- 16 P. E. Blöchl, Phys. Rev. B: Condens. Matter Mater. Phys., 1994, 50, 17953-17979.
- 17 G. Kresse and D. Joubert, Phys. Rev. B: Condens. Matter Mater. Phys., 1999, 59, 1758-1775.

- 18 J. P. Perdew, K. Burke and M. Ernzerhof, Phys. Rev. Lett., 1996, 77, 3865-3868.
- 19 J. E. Saal, S. Kirklin, M. Aykol, B. Meredig and C. Wolverton, JOM, 2013, 65, 1501-1509.
- 20 Low spin ferromagnetic ordering was also considered, but the calculations always converged to the high spin state.
- 21 D. E. Bugaris and H.-C. zur Loye, Angew. Chem., Int. Ed., 2012, 51, 3780-3811.
- 22 R. M. Barrer and E. A. D. White, J. Chem. Soc., 1951, 1267-1278.
- 23 P. Feng, X. Bu, S. H. Tolbert and G. D. Stucky, J. Am. Chem. Soc., 1997, 119, 2497-2504.
- 24 M. Andratschke, K.-J. Range, C. Weigl, U. Schiessl, F. Z. Rau and B. Naturforsch, J. Chem. Sci., 1994, 49, 1282-1288.
- 25 H. Y. Ng and W. T. A. Harrison, Microporous Mesoporous Mater., 1998, 23, 197-202.
- 26 P. F. Henry and M. T. Weller, Chem. Commun., 1998, 2723-2724.
- 27 B. M. Gatehouse, Acta Crystallogr., Sect. C: Cryst. Struct. Commun., 1989, 45, 1674.
- 28 C. A. Juillerat, V. Kocevski, T. M. Besmann and H.-C. zur Loye, Inorg. Chem., 2019, 58, 4099-4102.
- 29 H.-X. Deng, J. Li, S.-S. Li, J.-B. Xia, A. Walsh and S.-H. Wei, Appl. Phys. Lett., 2010, 96, 162508.